Resistant Mechanism against Nelfinavir of Human Immunodeficiency Virus Type 1 Proteases

Hirotaka Ode, Masami Ota, Saburo Neya, Masayuki Hata,Wataru Sugiura†, Tyuji Hoshino*

Graduate School of Pharmaceutical Sciences, Chiba University, Chiba 263-8522, Japan

TITLE RUNNING HEAD: Resistant Mechanism against NFV of HIV-1 PR.

CORRESPONDING AUTHOR FOOTNOTE

* Corresponding author. Tel: +81-43-290-2926. Fax: +81-43-290-2925.

Email: odehir@graduate.chiba-u.jp

† AIDS Research Center, National Institute of Infectious Diseases, Musashimurayama, Tokyo 208-0011, Japan.

ABSTRACT Inhibitors against human immunodeficiency virus type-1 (HIV-1) proteases are finely effective for anti-HIV-1 treatments. However, the therapeutic efficacy is reduced by the rapid emergence of inhibitor-resistant variants of the protease. Among patients who failed in the inhibitor nelfinavir (NFV) treatment, D30N, N88D, and L90M mutations of HIV-1 protease are often observed. In spite of the serious clinical problem, it is not clear how these mutations, especially non-active site mutations N88D and L90M, affect the affinity of NFV and/or why they cause the resistance to NFV. In this study, we executed molecular dynamics simulations of the NFV-bound proteases in the wild-type and D30N, N88D, D30N/N88D, L90M mutants. Our simulations clarified the conformational change at the active site of the protease and the change of the affinity with NFV for all of these mutations, even though the 88th and 90th residues are not located in the NFV-bound cavity and not able to directly interacts with NFV. D30N mutation causes the disappearance of the hydrogen bond between *m*-phenol group of NFV and the 30th residue. N88D mutation alters the active-site conformation slightly, and induces a favorable hydrophobic contact. L90M mutation dramatically changes the conformation at the flap region and leads to an unfavorable distortion of the binding pocket of the protease, although 90M is largely far apart from the flap region. Furthermore, the changes of binding energies of the mutants from the wild-type protease are shown to be correlated with the mutant resistivity previously reported by the phenotypic experiments.

KEYWORDS HIV-1 protease; nelfinavir; drug resistance; MD simulation; conformational change; non-active site

Introduction

Replication of human immunodeficiency virus type 1 (HIV-1) requires the processing of gag and gag-pol polyprotein precursors by the virus-encoded aspartic protease, so called HIV-1 protease.[1] Therefore the protease has been one of the major targets of anti-HIV-1 treatments.[2] Today, seven protease inhibitors (PIs) are approved by FDA and available clinically. Those drugs are well designed to fit the inside of the binding cavity, mimicking the configuration of a substrate in the transition state for the hydrolysis reaction by the protease.[3] However, HIV-1 frequently acquires the resistance to these inhibitors through specific mutations due to the high polymorphism and adaptability of the protease.[4-7] Serious resistant mutants survive during the treatment with PIs, and cause a failure in long-term HIV chemotherapy.

Among patients who failed in the treatment with nelfinavir: NFV (Figure 1), which is one of PIs, substitutions of asparagine (N) for aspartic acid (D) at codon 30 (D30N), aspartic acid for asparagine at codon 88 (N88D), and methionine (M) for leucine (L) at codon 90 (L90M) are frequently seen in HIV-1 protease.[8,9] D30N is a primary NFV-resistant mutation, which appears to be very specific for this inhibitor. N88D is an additional mutation to D30N. A combination of D30N and N88D is the most commonly seen in patients treated with NFV, and N88D compensates for the loss of replicative capacity resulting from D30N, as a secondary mutation. L90M is a primary mutation responsible for the resistance to both NFV and saquinavir,[10] and also appears to be associated with the resistance to the other PIs.[4-6] There are two evolutionally possible pass ways for the NFV-related mutation acquisition, and the L90M acquisition pass way is evolutionally different from the pass way of D30N.[11,12]

The three-dimensional X-ray structure of the NFV-bound protease[13] implies that D30N mutation would alter the direct electrostatic interaction with *m*-phenol group of NFV at the active site (Figure 2). It is, however, difficult to understand the NFV-resistance due to N88D or L90M mutations because these 88th, 90th residues are located at the non-active site near the dimer interface. Recently, Mahalingam and coworkers determined some high resolution X-ray crystal structures of D30N, N88D, or L90M mutants combined with peptide inhibitor analogues, not NFV[14-16], and suggested the mechanism of the resistance. They found that D30N mutation altered the interaction with the inhibitors, N88D mutation lost the water that mediated hydrogen bond interactions among 31T, 74T, and 88D, and L90M caused an unfavorable van der Waals contact between 24T/25D and the long side chain of 90M. Further, they reported that L90M mutants altered the active site conformation when indinavir entered the binding cavity of the protease.[17] Though these structural features might be seen in the proteases

complexed with NFV, a clear explanation on the resistance to NFV due to these mutations has not been provided yet.

Computational chemistry has been developed in recent years and detailed analysis has been significantly improved. Many computational works were already carried out to clarify catalytic mechanism of HIV-1 protease in its substrate-hydrolysis reaction.[18-30] And the other works discussed the drug-resistant mechanisms of some familiar active site mutations.[31-36] In the present study, we discussed the resistant mechanism of not only active site mutation D30N, but also non-active site mutations N88D, L90M. In order to clarify these mechanisms, we investigated the wild-type HIV-1 protease and D30N, N88D, D30N/N88D, L90M mutants complexed with NFV based on molecular dynamics (MD) approach explicitly including the solvate condition. Our MD simulations for each mutant demonstrated the respective resistant mechanisms to NFV. Not only active site mutation D30N but also non-active site mutations N88D, L90M affect the interaction between NFV and the protease through the structural modification of the binding cavity. There are no papers reported on the resistant mechanism of the non-active site mutations through a computational approach. The atom-level understanding of the origins of these resistances will be useful in the design of better protease inhibitors. Further, our work suggests the possibility to reproduce the experimental phenotype data from the results of MD simulation.

Materials and methods

Molecular Dynamics Simulation

The reliability of MD simulations largely depends on the selection of force field parameters and the assignment of atomic charges. Hence, the electrostatic potential of NFV was preliminarily calculated at the B3LYP/6-31G(d, p) level using Gaussian98 program[37] after geometry optimization. The partial atom charges for NFV utilized in MD simulation were determined using RESP method[38] so that the atom charges could reproduce the values of the calculated electrostatic potential at the surrounding points of NFV. The charges were set equal between two atoms if they are the same element and have the same bond coordination. Afterward, all the minimizations and molecular dynamics simulations were executed with Sander module of AMBER7 package.[39] The AMBER parm99 force field[40] was used as the parameters for van der Waals and the bonded energy terms.

Each initial structure for the wild-type protease of clade B and D30N, N88D, D30N/N88D, L90M mutants complexed with NFV was modeled based on the coordinates of an X-ray crystal structure

(PDB code: 1OHR[13]) using LEaP module. All the crystal waters were included in each model. Each model was placed in a periodic cubic box filled with the about 8,000 TIP3P water molecules.[41] The cut off distance for the long-range electrostatic and the van der Waals terms was 12.0 Å. All covalent bonds to hydrogen atom were constrained using the SHAKE algorithm.[42] Periodic boundary conditions were applied to avoid the edge effects in all calculations. Energy minimization was achieved via three stages. At first, the movement was allowed only for the water molecules. Next, the ligand and the mutated residues were allowed to move in addition to the water molecules. At last, all atoms were permitted to move freely. In each stage, energy minimization was executed by the steepest decent method for the first 1,000 steps and the conjugated gradient method for the subsequent 3,000 steps. The protonation states of the catalytic aspartates 25D/25'D were determined performing energy minimizations for all combinations of the protonation states (25D/25'D both protonated, 25D/25'D both unprotonated, 25D protonated and 25'D unprotonated, 25D unprotonated and 25'D protonated). The combination with protonated 25D and unprotonated 25'D showed the lowest total potential energy. This protonation state is consistent with the results of the previous work by Zoete et al.[43]

After 24 ps heating calculation until 300K using NVT ensemble, MD simulations were executed using NPT ensemble at 1 atm and at 300K for more than 1 ns, with a basic time step of 1 fs. After 500 ps equilibrating calculation, the MD simulations showed no large fluctuations (the deviation of RMSD of main chain is less than 0.1 Å in each model. More detail data is shown in Supporting Information). Coordinates of 200 snapshots at the interval of 0.5 ps were obtained as structural data, those were collected for the last 100 ps of the simulations.

Difference Distance Plot

The difference distance plots are drawn to assess the intermolecular relative shifts in response to the mutation. Firstly, $\mathbf{C\alpha i}$-to-$\mathbf{C\alpha j}$ distances, $\mathbf{d_{ij}^{A}}$, are computed for all the combinations of the $\mathbf{C\alpha}$ atoms in the protease of a mutant (A). Secondly, the same distances, $\mathbf{d_{ij}^{B}}$, are measured for the wild-type model (B). The difference distances $\mathbf{D_{ij}^{AB}}$ of the residue $\mathbf{i}$ and $\mathbf{j}$ is given by

$$\mathbf{D_{ij}^{AB}} = \left| \mathbf{d_{ij}^{A}} - \mathbf{d_{ij}^{B}} \right|$$

Further, the error-scaled difference distance[44,45] $\mathbf{E_{ij}^{AB}}$ is estimated by

$$\mathbf{E_{ij}^{AB}} = \mathbf{D_{ij}^{AB}} \Big/ \sigma\left(\mathbf{D_{ij}^{AB}}\right)$$

$$\sigma\left(\mathbf{D}_{ij}^{AB}\right) = \left[\left(\sigma_{r,i}^{A}\right)^2 + \left(\sigma_{r,j}^{A}\right)^2 + \left(\sigma_{r,i}^{B}\right)^2 + \left(\sigma_{r,j}^{B}\right)^2\right]^{1/2}$$

where $\sigma_{r,i}^{A}$ is the radial positional error that corresponds to the uncertainty for individual atom position. The difference distance is plotted on the lower left triangle, and the error-scaled difference distance is on the upper right one in the two dimensional map of Figure 4 as a function of residue numbers by using GNUPLOT.[46]

Hydrogen Bond Criterion

The formation of a hydrogen bond was defined in terms of distance and orientation. The combination of donor D, hydrogen H, and acceptor A atoms with a D - H … A configuration is regarded as a hydrogen bond when the distance between donor D and acceptor A is shorter than $\mathbf{R}_{max}$ and the angle H-D-A is smaller than Θ_{max}. 3.5 Å and 60.0° were adopted for $\mathbf{R}_{max}$ and Θ_{max} in this study.

Buried Surface Area

The solvate accessible surface area: SA[47] was computed with Paul Beroza's molsurf program, which was based on the analytical technique primarily developed by Connolly[48] in order to evaluate the surface area buried by a ligand in binding to the enzyme. SA is computed for the NFV-bound protease structure. SA is also calculated both for only NFV and for the free protease. The difference in SA value between the bound and unbound cases is defined as the surface area buried on complexation.[49]

Binding Energy Calculation

The binding free energy[50] is calculated based on the next equation:

$$\Delta G_b = \Delta G_{MM} + \Delta G_{sol} - T\Delta S$$

where ΔG_b is the binding free energy in solution, ΔG_{MM} is the interaction energy between the ligand and the protein, ΔG_{sol} is the solvation energy, and $-T\Delta S$ is the conformational entropy contribution to the binding. Assumed that the entropies are almost same in magnitude among the mutants, the difference in entropy is disregarded in the comparison of the binding energy in this study. ΔG_{MM} is calculated from molecular mechanics (MM) interaction energy:

$$\Delta G_{MM} = \Delta G_{int}^{ele} + \Delta G_{int}^{vdw}$$

where ΔG_{int}^{ele} and ΔG_{int}^{vdw} are electrostatic and van der Waals interaction energies between a ligand and a protein. These energies are computed using the same parameter set with the simulation, and no cut off is applied for the calculation. Solvation energy ΔG_{sol} can divide into to the two parts:

$$\Delta G_{sol} = \Delta G_{sol}^{ele} + \Delta G_{sol}^{nonpol}$$

The electrostatic contribution to the solvation free energy (ΔG_{sol}^{ele}) is calculated with the Poisson-Boltzmann (PB) method using DelPhi program.[51] The hydrophobic contribution to the solvation free energy (ΔG_{sol}^{nonpol}) is determined with a function of the solvent-accessible surface-area.[52]

Results

Conformational changes of the protease

In order to study the mechanism of the drug resistance, we compared the averaged atom coordinates of the wild-type with those of each mutant. The least-squared rigid body superposition indicates that no large conformational alteration appears in the shape of the protease for every mutant, as shown in the left column of Figure 3. The root-mean square deviation (RMSD) measurement was executed by using the coordinates of backbone atoms N, Cα, C in the superimposed structures of the wild-type and each mutant. RMSD value compared with the wild-type model is 0.8 Å in D30N, 0.9 Å in N88D, 1.1 Å in L90M, and 0.6 Å in D30N/N88D mutant model, averaged over the whole structure. The detailed analysis of individual residues and the comparison of the local structures, however, provided new understanding on the conformational changes due to the mutation. Although large deviations are seen at the residues of the outside loop region, those residues are not minutely examined because their large fluctuations are commonly observed irrelevant to the mutations in B-factor analysis.[43,53] The most characteristic conformational change is detected in the L90M mutant structure. The L90M mutant structure of our study displays significant backbone deviations at the flap regions (43K-58Q, 43'K-58'Q) and at the 79'P loop (78'G-84'I). RMSD values are 1.6 Å at the flap of one subunit, 2.0 Å at the opposite flap, and 1.9 Å at the 79'P loop. Those values are very large compared with those of the other mutants (0.5 Å / 0.6 Å / 0.7 Å in D30N, 0.6 Å / 0.7 Å / 0.7 Å in N88D, 0.5 Å / 0.6 Å / 0.5 Å in D30N/N88D). It should be emphasized that, though the 90th residue is not located at the flap nor at the 79'P loop, L90M affects the conformation at those regions. In N88D mutant structure, peculiar conformational changes occur at the β-sheets consisting of 59Y-75V (RMSD: 1.4 Å) and 59'Y-75'V (RMSD: 1.2 Å). Those regions move far away from the helix region (87R-90L / 87'R-90'L).

D30N/N88D mutant structure exhibits the similar conformational changes at the same but much narrow regions of those β-sheets; 74T/74'T and its vicinity.

In order to interpret small and more detailed conformational differences, we compared pairwise Cα-Cα distances in the averaged coordinates of each mutant model with those of the wild-type. Each difference distance is shown in the lower left triangle of the map in Figure 4, and the upper right triangle shows the error-scaled difference distance.[44,45] Figure 4 also indicates that L90M model has large conformational changes at the flap region (50I/50'I and its vicinity) and at the loop region at 79'P. N88D and D30N/N88D models alter the conformations at the β-sheets (74'T and its vicinity). In addition, these maps provide more detailed comprehension. The flap conformational alteration in L90M mutant is owing to the approach of 50I to the triads (25D26T27G / 25'D26'T27'G) and the detachment of 50'I from the triads. 79'P, 81'P, and some residues at the same loop are far apart from the residues at the opposite subunit. This loop moves outward and also makes a distance from NFV. The mutants other than L90M exhibit the common structural alteration. For example, the distance between the triad and the flap region is slightly changed. The RMSD from the wild-type at the triads in each subunit is 0.8 Å / 1.0 Å (D30N), 0.8 Å / 1.2 Å (N88D), 0.8 Å / 1.1 Å (D30N/N88D). These deviations are much larger, compared to RMSD at the flap region. Hence, characteristic distortion in D30N, N88D, and D30N/N88D is mainly caused by the conformational change of the triad.

The above conformational changes were seen in the last 100 ps simulations. In order to ensure that these changes were not just from the local fluctuations of MD simulations, we examined the coordinates for the last 500 ps simulations. The analysis of the last 500 ps simulations brought us similar results about the conformational changes. L90M had large deviations at the flap (RMSD: 1.5 Å/1.8 Å) and at the 79'P loop (1.7 Å), compared with wild type structure. N88D mutation induced the conformational change at the β-sheets around 74T/74'T. In N88D, RMSD values of the β-sheets are 1.4 Å and 1.2 Å in each subunit. And In D30N/N88D, those are both 0.9 Å. Furthermore, RMSD values at the triads are 0.8 Å / 1.1 Å in D30N, 0.7 Å / 1.1 Å in N88D, and 0.8 Å / 1.1 Å in D30N/N88D.

Hydrophilic interactions between NFV and the protease

In protease-ligand interactions, hydrogen bonds play a crucial role in stabilizing the complex. Hydrogen bonds between the protease and NFV in every model are listed in Table 1. Analysis of the protease-NFV hydrogen bonds suggests that mutation has obviously affected the protease-NFV

hydrogen bond network. Only a few residues are responsible for the hydrogen bonds with NFV. Hydrogen bond networks consists of 25D/25'D (catalytic aspartates), 50I/50'I, 30D, 29'D, some water molecules, and NFV. The direct interaction between carboxyl group of 25'D and central hydroxyl group of NFV is very frequently seen in every model, whereas the protonated aspartate 25D hardly interacts with NFV, except for L90M model. At S2 pocket, main chain of 30D interacts with *m*-phenol group of NFV. In the wild-type, main chain of 30D directly interacts with NFV. In each of N88D and L90M models, one water molecule links 30D and NFV with a hydrogen bond chain although the distance between the donor and acceptor atoms is elongated. On the other hand, no hydrogen bond is observed in the mutated D30N and D30N/N88D models. D30N mutation causes the disappearance of hydrogen bond network at S2 pocket, because those mutants increase the distances with the *m*-phenol group of NFV and cannot keep any water molecule. At the flap region, one water molecule exists at the neighbor of 50I and/or 50'I and NFV in all models. This water intermediates the intra-molecular and inter-molecular hydrogen bonds, which results in stabilizing the protease-NFV complex. In the wild-type model, the water links main chain of 50'I with NFV. Further, a direct hydrogen bond between sulfur atom of NFV and main chain of 50I is detected and no water molecule mediates the hydrogen bond from 50I. In contrast, the water mediates the hydrogen bond between NFV and both 50I/50'I in the D30N model. NFV forms a hydrogen bond network with either 50I or 50'I in the other models (L90M, N88D, D30N/N88D). Both NFV and the water molecule hardly interacts with main chain of 50'I in L90M mutant, and with main chain of 50I in N88D, D30N/N88D mutants. Hence, each of N88D and L90M mutations weakens the hydrogen bond networks around 50I and 50'I respectively. Interestingly, a water molecule mediating a hydrogen bond with 29'D in S2 pocket is frequently observed in the simulations of D30N and L90M mutants. Another water molecule mediating an intra-molecular hydrogen bond in NFV is located near the catalytic aspartates in both the wild-type and D30N models (WAT208 and WAT207 respectively). In the wild-type model, this water simultaneously mediates the hydrogen bond between 25'D and NFV.

In addition to the NFV-protease interaction at the active site, N88D mutation modulates the hydrogen bond network at the surroundings of the 88th residues (Figure 5). In the wild-type, main chain of 88N has a direct hydrogen bond with main chain of 29D, and side chain of 88N interacts with side chain of 31T. Those hydrogen bonds are also observed in the opposite subunit. Further, one water molecule links 88N with 74T (occupancy is 93.5 %) and 88'N with 74'T (75.5 %). In each of D30N and L90M, 88th residues in both subunit also have same hydrogen bond networks with 29th, 31st, and 74th

residues. But in N88D and D30N/N88D mutant, the water-mediated hydrogen bond does not exist. That is, N88D mutation induces the disappearance of the hydrogen bonds mediated by water molecules, though the direct hydrogen bonds are retained.

Hydrophobic interactions between NFV and the protease

Hydrophobic interactions and van der Waals interactions also contribute to stabilizing the complex. We evaluated the surface area buried by the complexation, which is related with the hydrophobicity of the binding cavity and the magnitude of van der Waals contacts between ligand and enzyme.[54-56] The results in Table 2 and Figure 6 show that most of the buried residues are hydrophobic ones. The 2-methyl-3hydroxylbenzamide moiety of NFV has hydrophobic contacts with 23L, 28A, 84I of the protease at S2 pocket, and the *tert*-butylcarboxamide moiety has contacts with 32'V, 47'I at S2' pocket. Hydrophobic interactions are also seen between dodecahydroisoquinoline ring and 23L, 28A, 81P, 82V, 84I, 50'I of the protease at S1 pocket, and between the S-phenyl group and 50I, 23'L, 28'A, 81'P, 82'V, 84'I at S1' pocket. The stabilization caused by hydrophobic interaction is mainly due to 50I/50'I, 84I/84'I, and secondly 28A/28'A, 48G/48'G and 81'P. L90M mutant hardly has hydrophobic contacts with NFV at 48'G and 81'P. This little hydrophobic contributions at 48'G and 81'P result in the serious decrease of the buried surface. D30N mutation hardly affects the buried surface area, whereas N88D mutation increases the buried surface area.

Binding energy calculation

Table 3 shows the binding energy between NFV and protease. Each mutation causes a distinctive energetical change from the wild-type. D30N decreases the electrostatic energy greatly. N88D becomes more stable due to the electrostatic contribution by solvation effect than the wild-type. D30N/N88D model has both characters of D30N and N88D models. D30N/N88D is less stable than N88D due to the electrostatic contribution and is more stable than D30N by the solvation effect. L90M causes a decrease of the electrostatic energy and a large decrease of the van der Waals energy. These energetical results are compatible with the indices of resistance level that were estimated from experimental IC90.[8,9]

Discussion

We executed molecular dynamics simulations to understand the resistance mechanism against NFV about not only active site mutation D30N, but also N88D, L90M. The simulations suggest that these

mutations affect the protease structures on complexation and the NFV-protease interactions, in spite of the location of the mutated residues.

D30N is a primary mutation of NFV, which emerges during the treatment with this inhibitor highly specifically. The X-ray crystal structure of the wild-type protease complexed with NFV[13] shows that *m*-phenol group of NFV interacts with both main chain atoms and side chain carboxyl group of 30D at S2 pocket. Accordingly, D30N mutation has been assumed to make less hydrophilic contacts and causes the disappearance of the hydrogen bond interaction from the 30th residue.

Clemente et al. investigated D30N mutant protease using docking study previously.[33] They concluded that D30N mutant would maintain the hydrogen bond between 30N and NFV, but weakens the strength of hydrogen bonding due to the decrease of acid-base interaction. However, their computational model could move only nelfinavir and side chain of 30N in the vacuum condition without any water molecules. That is, their docking simulations didn't consider the contributions of the movement of the residues other than 30N nor water solvation effects. MD simulation is useful to incorporate these contributions and to provide more detailed information. The proton or water-mediated hydrogen bonds are observed between *m*-phenol group of NFV and main chain of 30D in the wild-type model and the other models having a sequence of 30D, although side chain carboxyl oxygens of 30D has no hydrogen bond with NFV. D30N cancels those hydrogen bonds and decreases the electrostatic interaction energy greatly. In addition, we find that D30N mutation loses an ability to keep any water molecule at S2 pocket. Then, the substitution of asparagine (N) for aspartate (D) at codon 30 is concluded to cause NFV-resistance due to the serious decrease in the electrostatic interaction.

N88D is known as a secondary mutation for NFV and frequently seen in clinical scene next to D30N. Because the 88th residue is located at the helix region near the dimer interface, not at the active site, it is not clear why N88D substitution affects the resistance against NFV. Mahalingam and coworkers determined the X-ray crystal structure of N88D mutant with substrate analogue inhibitors, not NFV.[14-16] They found that 88N in the wild-type had the proton and/or water-mediated interactions with 29D, 31T, and 74T in each subunit, whereas the corresponding water molecules were missing in both subunits of N88D single mutant. It is also found from our calculation on the wild-type protease that the side chain of 88N makes a hydrogen bond network with 74T via one water molecule, the backbone nitrogen of 88N has a hydrogen bond with 29D, and side chain oxygen of 88N interacts with 31T. These hydrogen bond networks are also observed in the opposite subunit. In contrast, in each of N88D and D30N/N88D mutants, 88D interacts with only 31T and 29D, and the hydrogen bond

mediating water molecules disappear in the respective subunit. That is, the 88th residue cannot form any hydrogen bond with the 74th residue. This disappearance of the water-mediated hydrogen bond allows a large conformational change at the 74th residue. The conformational change at the β-sheet consisting of the 74th residue and its adjacent contiguous residues induces the conformational changes at the neighboring β-sheet and at the outside loop neighbor to the 74th residue. Further, we have detected that the slight conformational change of the NFV binding pocket due to N88D mutation induces the increase of hydrophobic contacts between NFV and the protease. The loss of the interaction between 74T and 88D would lower the constraint at 29D, 31T, and 74T, which results in the slight conformational change of the active site. Energetical analysis evidently indicates this increase of hydrophobicity. Consequently NFV is stabilized by the increase of hydrophobic effects when N88D is acquired, while D30N/N88D destabilizes NFV by a large loss of electrostatic interaction. The reduction of the constraint might induce the compensation for the loss of replicative capacity resulting from D30N, and keep the binding affinity with substrates, while the resistance against NFV is retained.

90L/M is also located at the helix region near the dimer interface, not at the active site. L90M mutants complexed with a substrate analogue inhibitor, not NFV, were also investigated by Mahalingam and coworkers.[14-16] They concluded that L90M altered van der Waals interactions in the hydrophobic interior at the dimer interface near the catalytic aspartates, and 90L related with the stability of the dimer. We also find the alteration of van der Waals interactions in L90M model. Side chains of the 90th residues are close to side chains of 24L/24'L and main chain of 25D/25'D (Figure 7-A). A methionine has a long and straight side chain, while a leucine has a diverging side chain. The substitution of methionine for leucine makes a collision of the 90th residues with 24L/24'L and 25D/25'D. This causes the conformational change at the triads. The conformational change of the triads induces large conformational changes at the flap and at the loop near the 79'P-81'P due to the presence of NFV (Figure 7-B). Those regions are surprisingly very far apart from the 90th residue. In L90M mutant, the conformation in the binding pocket is greatly changed. Especially, the loop region moves outward from NFV and make a large gap, therefore, the van der Waals and hydrophobic energies decrease greatly. The character of this conformational change resembles the conformational change of the indinavir-bound L90M protease[17] and the saquinavir-bound G48V/L90M protease.[57] The reason for the multi-drug resistance relevant to L90M mutation would be the conformational change of the triads and subsequent these hydrophobic at the flap and 79'P loop. The flap and loop region interacts with each of the dodecahydroisoquinoline ring of NFV, the pyridyl group of indinavir, and the planar quinoline

group of saquinavir. Those chemical bases are the largest in each inhibitor, and are very bulky compared with the protease substrates. No structural distortion appears at the loop region of the L90M complexed with the substrate analogue inhibitors. Therefore, it is speculated that the structural distortion seen in the inhibitor-bound L90M mutants is due to the largeness of quinoline ring or pyridyl group in volume. Then, in order to reduce and/or eliminate the resistance of L90M, the moiety that interacts with the loop region should be less bulky.

Our molecular dynamics studies indicate that the drug-resistant mutations affect the conformations of the binding cavity and the hydrophilic and hydrophobic interactions at the active site, even though the location of mutated residues is apart from the active site.

Furthermore, the difference in the binding energy between the wild-type model and those of each mutant are compatible with the indices of resistance level that were estimated from experimental IC90.[8,9] In present, there exist some computational approaches to explain the phenotype results.[32,35,58,59] Although every of them successfully predicted the decrease of the binding affinity in case of the active site mutation, they failed in the prediction of the non-active site mutation as L90M. Computational prediction is usually based on the assumption that PI resistance is primarily determined by a reduction in binding affinity. Therefore, the previous studies proposed that the drug-resistance due to the non-active site mutation might be caused by other mechanism, such as decreasing the dimer stability of the protease.[57,60] However, our study indicates that the assumption is applicable to the non-active site mutation. Some non-active site residues without any direct contact with inhibitors (e.g. 10L, 46M, 90L) have a strong positional correlation with the residues located at the active site. Hence, the non-active site mutations would cause a displacement of the active site residues and the decrease of the inhibitor or substrate binding affinity. We suggest that evaluating the positions of all the residues in the mutated protease is a key factor for the success in computational prediction of the protease resistivity against protease inhibitors. Additionally, it is also applicable to the design in order to reduce and/or to eliminate the resistance at the non-active site mutations.

Conclusions

We executed molecular dynamics simulations for the wild-type and D30N, N88D, D30N/N88D and L90M mutants in order to clarify the resistant mechanism of each mutation against nelfinavir. Our results could reproduce the phenotype data, and clarified the conformational alterations at the active site and the interaction changes due to the mutation. D30N induces the disappearance of the hydrogen bond

between *m*-phenol group of NFV and the 30th residue, which results in the decrease of electrostatic binding energy. Further, D30N loses the ability to retain a water molecule at S2 pocket. N88D alters the conformation at the β-sheets consisting of 74T and its vicinity greatly. N88D also affects the active site conformation, which creates more favorable hydrophobic binding cavity. L90M affects the triads 25D26T27G and causes subsequent large conformational changes at the flap region and the 79'P loop, though the 90th residue is far apart from those regions. L90M decreases the van der Waals binding energy greatly.

ACKNOWLEDGMENT

This work was supported by the Health and Labor Science Research Grant for Research on HIV/AIDS from Ministry of Health and Labor of Japan.

Supporting Information Available

RMSD of the main chain atoms compared with the X-ray crystal structure (Figure 1S). This material is available free of charge via the Internet at http://pubs.acs.org.

FIGURE CAPTIONS

Figure 1. Structure of nelfinavir. According to the crystal structure (PDB code: 1OHR), the *m*-phenol group of the 2-methyl-3-hydroxylbenzamide side chain of nelfinavir interacts with 30D by a hydrogen bonding in S2 pocket of HIV-1 protease. The *tert*-butylcarboxamide moiety occupies S2' subsite, S-phenyl group and dodecahydroisoquinoline ring fit into the hydrophobic S1 and S1' pocket, and the central hydroxyl group is bound to the catalytic aspartates.

Figure 2. X-ray structure of HIV-1 protease/nelfinavir complex (PDB code: 1OHR). Locations of the two catalytic aspartates, and the residues related with NFV resistance (30,88,90) are shown in the stick representation in one subunit of the protease dimer. The wild-type sequence is shown below.

Figure 3. Left: Plots of RMSD between the average structures of the wild-type protease and each mutant, traced over every main chain atoms. Each mutant structure is superimposed on the wild-type structure represented by white tube. Right: B-factor values for main chain atoms in the wild-type and mutated proteases. The color represents the magnitude of RMS and B-factor shown at the lower bar. Scales are in unit of Å and $Å^2$, respectively.

Figure 4. Difference distance matrices and error-scaled difference matrices for the Cα atoms. The difference distance for all pairs of residues in the protease is shown on the lower triangle. The color represents the magnitude shown at the bar in the lower left. The upper right triangle shows the error-scaled difference distance matrices. Changes greater than 1.0σ and smaller than 2.5σ are colored as seen on the lower right bar. Number 1-99 represents the residue from 1P to 99F, and number 101-199 represents the residue from 1'P to 99'F.

Figure 5. Hydrogen bond network surrounding the 88th residue. A: Wild-type protease structure. B: N88D mutant protease structure.

Figure 6. Buried surface areas due to each involved residue. The upper graph represents those of one subunit, and the lower graph is on the other subunit. L90M shows notable differences at 48'G, 81'P, 82'V from the other mutants.

Figure 7. Stereoview of the structures (A) at the surrounding region of the 90th residue and (B) at the flap region. The wild-type structure is represented by white tube and L90M mutant by blue tube.

TABLES

Table 1. Hydrogen bond network in each model.

		Hydrogen bond					
		Donor			Acceptor		Occupancy
Wild	catalytic domain	O21	-HOL	(NFV)	OD1	(25'D)	91.0%
		O21	-HOL	(NFV)	OD2	(25'D)	95.5%
		O	-H2	(WAT208)	O21	(NFV)	60.0%
		O	-H1	(WAT208)	OD2	(25'D)	61.0%
		N22	-HNM	(NFV)	O	(WAT208)	59.5%
	S2 pocket	O38	-HO	(NFV)	O	(30D)	90.0%
		N	-H	(30D)	O38	(NFV)	64.5%
	flap region	N	-H	(50I)	S74	(NFV)	61.0%
		O	-H1	(WAT205)	O17	(NFV)	51.5%
		N	-H	(50'I)	O	(WAT205)	61.0%
D30N	catalytic domain	O21	-HOL	(NFV)	OD2	(25'D)	100.0%
		N22	-HNM	(NFV)	O	(WAT210)	85.0%
		O	-H1	(WAT210)	O21	(NFV)	52.5%
	flap region	O	-H2	(WAT207)	O17	(NFV)	76.5%
		O	-H1	(WAT207)	O25	(NFV)	89.0%
		N	-H	(50I)	O	(WAT207)	50.5%
		N	-H	(50'I)	O	(WAT207)	93.5%
	S2' pocket	N12	-HNC	(NFV)	O	(WAT4757)	94.5%
		N	-H	(29'D)	O	(WAT4757)	85.0%
		O	-H2	(WAT4757)	OD1	(29'D)	52.5%
N88D	catalytic domain	O21	-HOL	(NFV)	OD2	(25'D)	100.0%
	S2 pocket	O	-H1	(WAT3880)	O38	(NFV)	59.0%
		N	-H	(30D)	O	(WAT3880)	87.5%
		O	-H2	(WAT3880)	O	(30D)	97.5%
	flap region	O	-H2	(WAT203)	O17	(NFV)	79.5%

		O	-H1	(WAT203)	O25	(NFV)	95.0%
		N	-H	(50'I)	O	(WAT203)	100.0%
D30N/N88D	catalytic domain	O21	-HOL	(NFV)	OD2	(25'D)	96.5%
	flap region	O	-H2	(WAT205)	O25	(NFV)	98.5%
		O	-H1	(WAT205)	O17	(NFV)	97.5%
		N	-H	(50'I)	O	(WAT205)	96.5%
L90M	catalytic domain	O21	-HOL	(NFV)	OD2	(25'D)	100.0%
		OD2	-HD2	(25D)	O21	(NFV)	90.5%
	S2 pocket	O	-H1	(WAT3836)	O38	(NFV)	73.5%
		N	-H	(30D)	O	(WAT3836)	90.0%
		O	-H2	(WAT3836)	O	(30D)	99.5%
	flap region	O	-H2	(WAT205)	O17	(NFV)	96.5%
		O	-H1	(WAT205)	O25	(NFV)	97.5%
		N	-H	(50I)	O	(WAT205)	90.5%
	S2' pocket	N12	-HNC	(NFV)	O	(WAT4349)	93.5%
		N	-H	(29'D)	O	(WAT4349)	74.5%
		O	-H2	(WAT4349)	OD1	(29'D)	74.5%

The listed donor and acceptor pairs satisfy the criteria for the hydrogen bond over 50.0% of time during the last 100 ps simulation. Nomenclature of atoms is the same as that of 1OHR.

Table 2. Buried surface area and the contribution of hydrophobic and hydrophilic residues.

	Buried surface area ($Å^2$)	Hydrophobic : Hydrophilic*
Wild	805.9	83.0 : 17.0
D30N	809.9	82.8 : 17.2
N88D	841.5	83.1 : 16.9
D30N/N88D	832.6	86.1 : 13.9
L90M	765.2	87.1 : 12.9

* Hydrophobic residue : Gly / Ala / Val / Leu / Ile / Met / Pro / Phe / Trp

Hydrophilic residue : Ser / Thr / Asn / Gln / Tyr / Cys / Lys / Arg / His / Asp / Glu

Table 3. Binding free energies of the wild-type and mutants.

	ΔG_{int}^{ele} (kcal/mol)	ΔG_{int}^{vdw} (kcal/mol)	ΔG_{sol}^{nonpol} (kcal/mol)	ΔG_{sol}^{ele} (kcal/mol)	$\Delta G_{int+sol}^{ele}$ (kcal/mol)	ΔG_b † (kcal/mol)	Resistance level*
Wild	-26.5±4.2	-66.4±3.3	-4.5±0.1	44.2±3.4	17.7±3.5	-53.2±4.2	-
D30N	-19.2±2.8	-64.0±2.8	-4.5±0.2	38.2±3.6	19.0±3.7	-49.5±3.5	6
N88D	-26.2±3.5	-66.0±3.5	-4.7±0.3	42.6±3.7	16.4±3.6	-54.3±3.9	0.6
D30N/N88D	-15.1±3.9	-64.9±3.3	-4.6±0.2	35.4±3.7	20.3±3.8	-49.2±4.0	6
L90M	-21.1±3.5	-62.2±3.0	-4.2±0.2	36.4±3.5	15.3±4.0	-51.2±4.0	5

* reference 8, 9 † $\mathbf{T\Delta S}$ is not included.

REFERENCES

(1) Kohl, N .E.; Emini, E. A.; Schleif, W. A.; Davis, L. J.; Heimbach, J. C.; Dixon, R. A.; Scolnick, E. M.; Sigal, I. S. *Proc. Natl. Acad. Sci. USA* **1988**, *85*, 4686.

(2) Debouck, C. *AIDS Res. Hum. Retroviruses* **1992**, *8*, 153.

(3) Roberts, N. A.; Martin, J. A.; Kinchington, D.; Broadhurst, A. V.; Craig, J. C.; Duncan, I. B.; Galpin, S. A.; Handa, B. K.; Kay, J.; Krohn, A.; Lambert, R. W.; Merrett, J. H.; Mills, J. S.; Parkes, K. E. B.; Redshaw, S.; Ritchie, A. J.; Taylor, D. L.; Thomas, G. J.; Machin, P. J. *Science* **1990**, *248*, 358.

(4) Johnson, V. A.; Brun-Vézinet, F.; Clotet, B.; Conway, B.; D'Aquila, R. T.; Demeter, L. M.; Kuritzkes, D. R.; Pillay, D.; Schapiro, J. M.; Telenti, A.; Richman, D. *Top. HIV Med.* **2003**, *11*, 215.

(5) Wu, T. D.; Schiffer, C. A.; Gonzales, M. J.; Taylor, J.; Kantor, R.; Chou, S.; Israelski, D.; Zolopa, A. R.; Fessel, W. J.; Shafer, R. W. *J. Virol.* **2003**, *77*, 4836.

(6) Kantor, R.; Fessel, W. J.; Zolopa, A. R.; Israelski, D.; Shulman, N.; Montoya, J. G.; Harbour, M.; Schapiro, J. M.; Shafer. R. W. *Antimicrob. Agents Chemother.* **2002**, *46*, 1086.

(7) Condra, J. H.; Schleif, W. A.; Blahy, O. M.; Gabryelski, L. J.; Graham, D. J.; Quintero, J. C.; Rhodes, A.; Robbins, H. L.; Roth, E.; Shivaprakash, M.; Titus, D.; Yang, T.; Teppler, H.; Squires, K. E.; Deutsch, P. J.; Emini, E. A. *Nature* **1995**, *374*, 569.

(8) Patick, A. K.; Duran, M.; Cao, Y.; Shugarts, D.; Keller, M. R.; Mazabel, E.; Knowles, M.; Chapman, S.; Kuritzkes, D. R.; Markowitz, M. *Antimicrob. Agents Chemother.* **1998**, *42*, 2637.

(9) Patick, A. K.; Mo, H.; Markowitz, M.; Appelt, K.; Wu, B.; Musick, L.; Kalish, V.; Kaldor, S.; Reich, S.; Ho, D.; Webber, S. *Antimicrob. Agents Chemother.* **1996**, *40*, 292. (Erratum, *40*, 1575)

(10) Jacobson, H.; Hängii, M.; Ott, M.; Duncan, I. B.; Owen, S.; Andreoni, M.; Vella, S.; Mous, J. *J. Infect. Dis.* **1996**, *173*, 1379.

(11) Sugiura, W.; Matsuda, Z.; Yokomaku, Y.; Hertogs, K.; Larder, B.; Oishi, T.; Okano, A.; Shiino, T.; Tatsumi, M.; Matsuda, M.; Abumi, H.; Takata, N.; Shirahata, S.; Yamada, K.; Yoshikura, H.; Nagai, Y. *Antimicrob. Agents Chemother.* **2002**, *46*, 708.

(12) Sugiura, W.; Oishi, T.; Okano, A.; Matsuda, M.; Abumi, H.; Yamada, K.; Koike, M.; Taki, M.; Ishikawa, M.; Miura, T.; Hukutake, K.; Gouchi, K.; Ajisawa, A.; Iwamoto, A.; Hanabusa, H.; Mimaya, J.; Takamatsu, J.; Takata, N.; Kakishita, E.; Higasa, S.,; Kashiwagi, S.; Shirahata, A.; Nagai, Y. *Jpn. J. Infect. Dis.* **1999**, *52*, 175.

(13) Kaldor, S. W.; Kalish, V. J.; Davies, J. F.; Shetty, B. V.; Fritz, J. E.; Appelt, K.; Burgess, J. A.; Campanale, K. M.; Chirgadze, N. Y.; Clawson, D. K.; Dressman, B. A.; Hatch, S. D.; Khalil, D. A.; Kosa, M. B.; Lubbehusen, P. P.; Muesing, M. A.; Patick, A. K.; Reich, S. H.; Su, K. S.; Tatlock, J. H. *J. Med. Chem.* **1997**, *40*, 3979.

(14) Mahalingam, B.; Boross, P.; Wang, Y.-F.; Louis, J. M.; Fischer, C. C.; Tozser, J.; Harrison, R. W.; Weber, I. T. *Proteins* **2002**, *48*, 107.

(15) Mahalingam, B.; Louis, J. M.; Hung, J.; Harrison, R. W.; Weber, I. T. *Proteins* **2001**, *43*, 455.

(16) Mahalingam, B.; Louis, J. M.; Reed, C. C.; Adomat, J. M.; Krouse, J.; Wang, Y.-F.; Harrison, R. W.; Weber, I.T. *Eur. J. Biochem.* **1999**, *263*, 238.

(17) Mahalingam, B.; Wang, Y.-F.; Boross, P. I.; Tozser, J.; Louis, J. M.; Harrison, R. W.; Weber, I. T. *Eur. J. Biochem.* **2004**, *271*, 1516.

(18) Piana, S.; Bucher, D.; Carloni, P.; Rothlisberger, U. *J. Phys. Chem. B* **2004**, *108*, 11139.

(19) Piana, S.; Parrinello, M.; Carloni, P. *J. Mol. Biol.* **2002**, *319*, 567.

(20) Trylska, J.; Bala, P.; Geller, M.; Grochowski, P. *Biophys. J.* **2002**, *83*, 794.

(21) Okimoto, N.; Kitayama, K.; Hata, M.; Hoshino, T.; Tsuda, M. *J. Mol. Struct. (Theochem.)* **2001**, *543*, 53.

(22) Okimoto, N.; Tsukui, T.; Kitayama, K.; Hata, M.; Hoshino, T.; Tsuda, M. *J. Am. Chem. Soc.* **2000**, *122*, 5613.

(23) Park, H.; Suh, J.; Lee, S. *J. Am. Chem. Soc.* **2000**, *122*, 3901.

(24) Okimoto, N.; Tsukui, T.; Hata, M.; Hoshino T.; Tsuda M. *J. Am. Chem. Soc.* **1999**, *121*, 7349.

(25) Ventrini, A.; López-Ortiz, F.; Alvarez, J. M.; Gonzalez, J. *J. Am. Chem. Soc.* **1998**, *120*, 1110.

(26) Liu, H.; Müller-Plathe, F.; Van Gusteren, W. F. *J. Mol. Biol.* **1996**, *118*, 3946.

(27) Weber, I. dT.; Harrison, R. W. *Protein Eng.* **1996**, *9*, 679.

(28) Harrison, R. W.; Weber, I. T. *Protein Eng.* **1994**, *7*, 1353.

(29) Beveridge, A. J.; Heywood, G. C. *Biochemistry* **1993**, *32*, 3325.

(30) Goldblum, A. *Biochemistry* **1988**, *27*, 1653.

(31) Perryman, A. L.; Lin, J.-H.; McCammon, J. A. *Protein Sci.* **2003**, *13*, 1108.

(32) Shenderovich, M. D.; Kagan, R. M.; Heseltine, P. N. R.; Ramnarayan, K. *Protein Sci.* **2003**, *12*, 1706.

(33) Clemente, J. C.; Hermrajani, R.; Blum, L. E.; Goodenow, M. M.; Dunn, B. M. *Biochemistry* **2003**, *42*, 15029.

(34) Piana, S.; Carloni, P.; Rothlisberger, U. *Protein Sci.* **2002**, *11*, 2393.

(35) Rick, S.W.; Topol, I.A.; Erickson, J.W.; Burt, S.K. *Protein Sci.* **1998**, *8*, 1750.

(36) Harte, W. E. Jr.; Beveridge, D. L. *J. Am. Chem. Soc.* **1993**, *115*, 1231.

(37) Frisch, M. J.; Trucks, G. W.; Scuseria, H. B.; Robb, M. A.; Cheeseman, J. R.; Zakrzewski, V. G.; Montgomery, J. A.; Stratmann, R. E.; Burant, J. C.; Dapprich, S.; Mllam, J. M.; Daniels, A. D.; Kudin, K. N.; Strain, M. C.; Farkas, O.; Tomasi, J.; Barone, V.; Cossi, M.; Cammi, R.; Mennucci, B.; Pommelli, C.; Adamo, C.; Clifford, S.; Ochterski, J.; Petersson, G. A.; Ayala, P. Y.; Cui, Q.; Morokuma, K.; Malick, D. K.; Rabuck, A. D.; Raghavachari, K.; Foresman, J. B.; Cioslowski, J.; Ortiz, J. V.; Stefanov, B. B.; Liu, G.; Liashenko, A.; Piskorz, P.; Komaromi, I.; Gomperts, R.; Martin, R.L.; Fox, D. J.; Keith, T.; Al-Laham, M. A.; Peng, C. Y.; Nanayakkara, A.; Gonzalez, C.; Challacombe, M.; Gill, P. M. W.; Johnson, B. G.; Chen, W.; Wong, M. W.; Andres, J. L.; Head-Gordon, M.; Replogle, E. S.; Pople, J. A. *Gaussian 98*; Gaussian, Inc.: Pittsburgh, PA, **1998**.

(38) Cieplak, P.; Cornell, W. D.; Bayly, C.; Kollman, P. A. *J. Comput. Chem.* **1995**, *16*, 1357.

(39) Case D. A.; Pearlman, D. A.; Caldwell, J. W.; Cheatham, T. E., III; Wang, J.; Ross, W. S.; Simmerling, C. L.; Darden, T. A.; Merz, K. M.; Stanton, R. V.; Cheng, A. L.; Vincent, J. J.; Crowley,

M.; Tsui, V.; Gohlke, H.; Radmer, R. J.; Duan, Y.; Pitera, J.; Massova, I.; Seibel, G. L.; Singh, U. C.; Weiner, P. K.; Kollman, P. A. *AMBER 7*; University of California: San Francisco, **2002**.

(40) Wang, J.;Cieplak, P.; Kollman, P. A. *J. Comput. Chem.* **2000**, *21*, 1049.

(41) Jorgensen, W. L.; Chandrasekhar, J.; Madura, J. D.; Impey, R. W.; Klein, M. L. *J. Chem. Phys.* **1983**, *79*, 926.

(42) Ryckaert, J.-P.; Ciccotti, G.; Berendsen, H. J. C. *J. Comput. Phys.* **1977**, *23*, 327.

(43) Zoete, V.; Michielin, O.; Karplus, M. *J. Mol. Biol.* **2002**, *315*, 21.

(44) Schneider, T. R. *Acta. Cryst.* **2002**, *D58*, 195.

(45) Schneider, T. R. *Acta. Cryst.* **2000**, *D56*, 714.

(46) Williams, T.; Kelley, C. *GNUPLOT* © 1986-1993, 1998 contact for further information http://www.gnuplot.info/, **1998**.

(47) Lee, B.; Richards, F. M. *J. Mol. Biol.* **1971**, *55*, 379.

(48) Connolly, M. L. *J. Appl. Cryst.* **1983**, *16*, 548.

(49) Prabu-Jeyabalen, M.; Nalivaika, E. A.; King, N. M.; Schiffer, C. A. *J. Virol.* **2003**, *77*, 1306.

(50) Kollman, P. *Chem. Rev.* **1993**, *93*, 2395.

(51) Honig, B.; Nicholls, A. *Science* **1995**, *268*, 1144.

(52) Sitkoff, D.; Sharp, K. A.; Honig, B. *J. Phys. Chem.* **1994**, *98*, 1978.

(53) Karplus, M.; Petsko, G. A. *Nature* **1990**, *347*, 631.

(54) Kuhn, L. A.; Siani, M. A.; Pique, M. E.; Fisher, C. L.; Getzoff, E. D.; Tainer, J. A. *J. Mol. Biol.* **1992**, *228*, 13.

(55) Chothia, C. *J. Mol. Biol.* **1976**, *105*, 1.

(56) Nozaki, Y.; Tanford, C. *J. Biol. Chem.* **1971**, *7*, 2211.

(57) Hong, L.; Zhang, X. C.; Hartsuck, J. A.; Tang, J. *Protein Sci.* **2000**, *9*, 1898.

(58) Jenwitheesuk, E.; Samudrala, R.. *BMC structural Biology* **2002**, *3*, 2.

(59) Wang, W.; Kollman, P. A.. *Pro. Natl. Acad. Sci.* **2001**, *98*, 14937.

(60) Xie, D.; Gulnik, S.; Gustchina, E.; Yu, B.; Shao, W.; Qoronfleh, W.; Nathan, A.; Erickson, J. W. *Protein Sci.* **1999**, *8*, 1702.

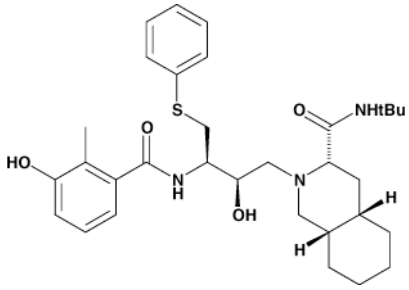

Ode et al. Figure 1.

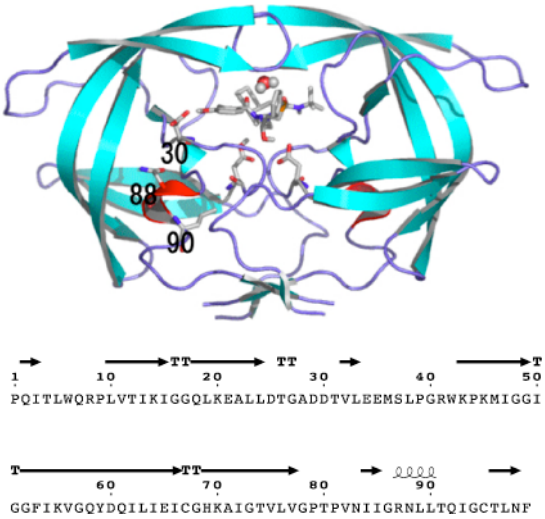

Ode et al. Figure 2.

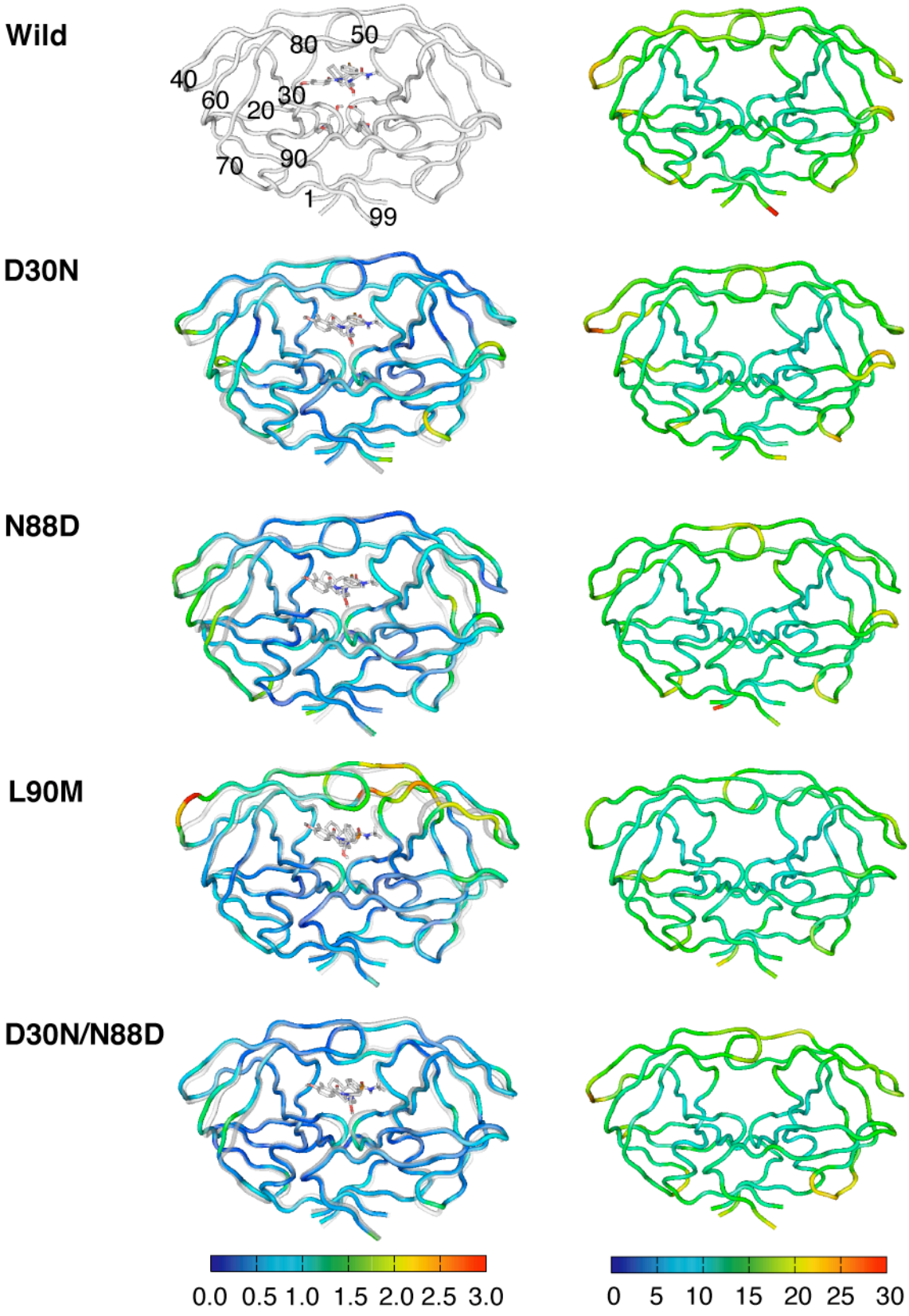

Ode et al Figure 3.

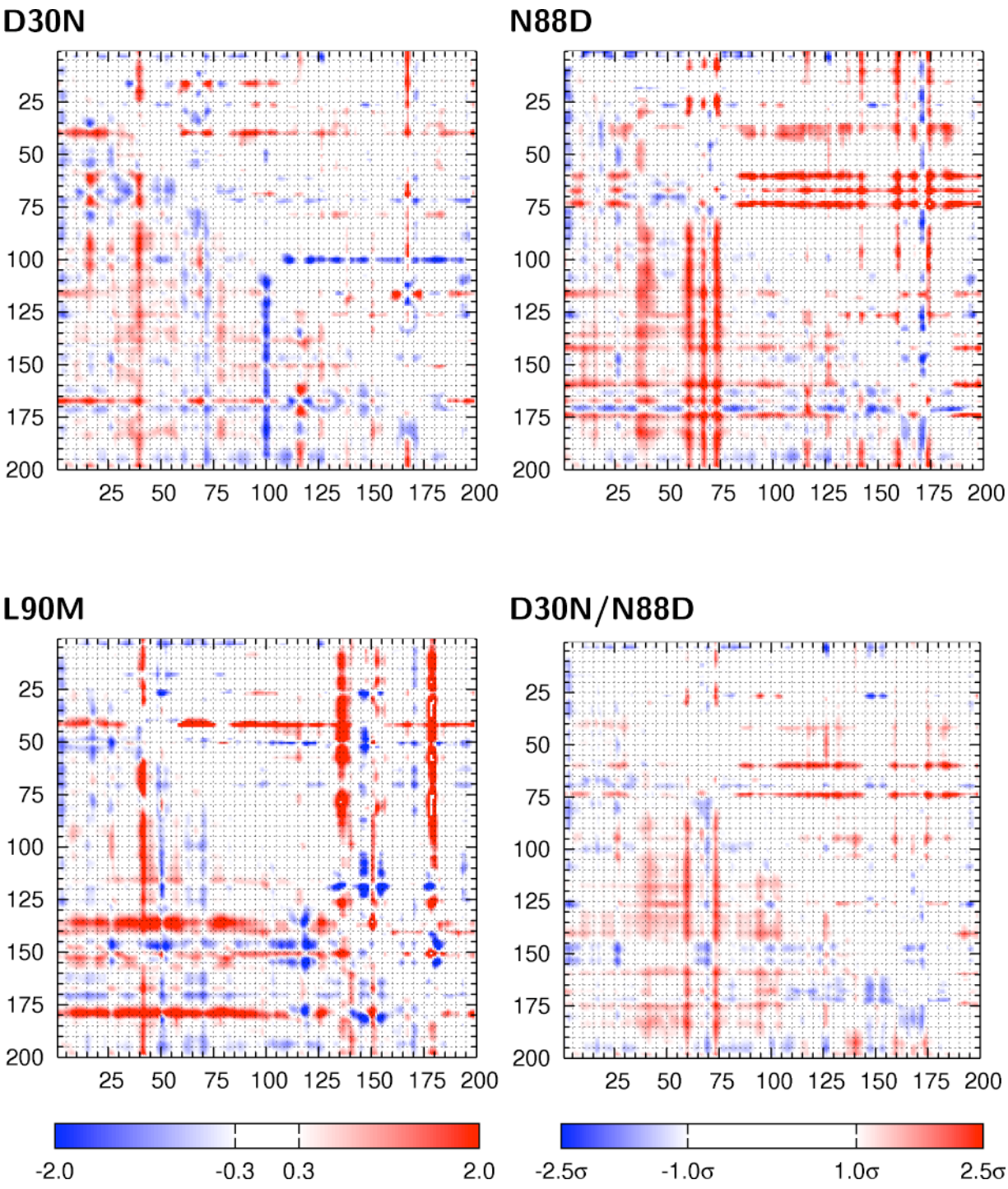

Ode et al. Figure 4.

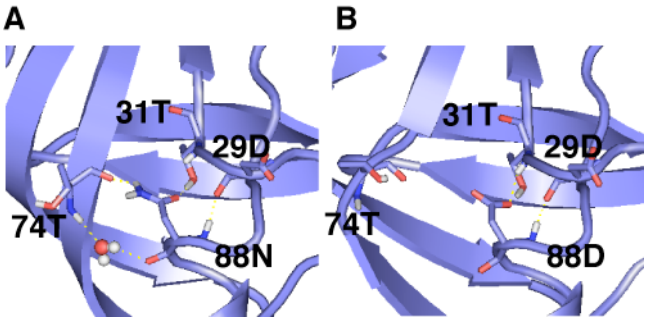

Ode et al. Figure 5.

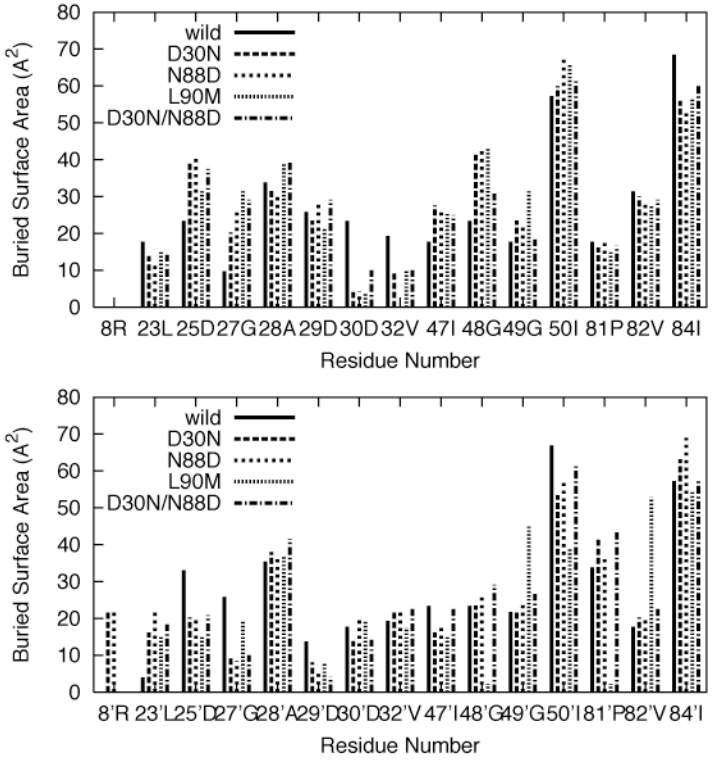

Ode et al. Figure 6.

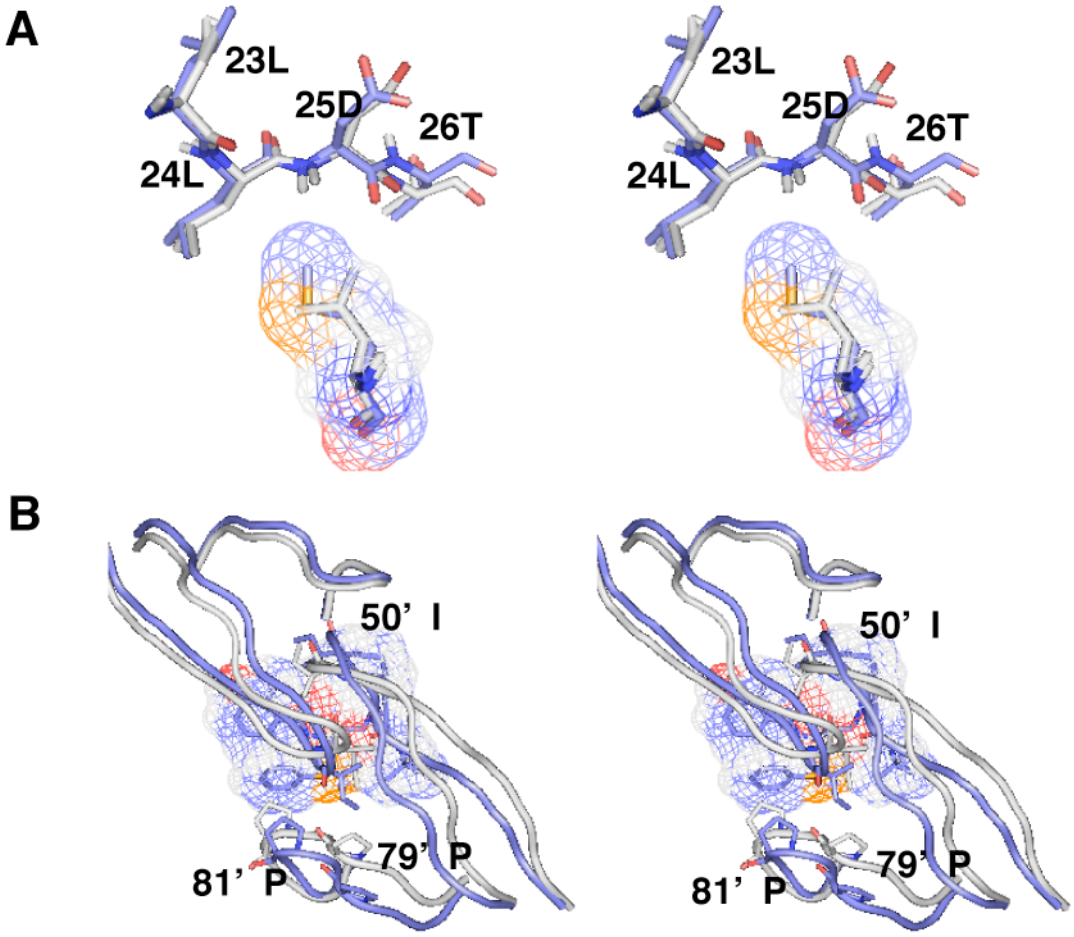

Ode et al. Figure 7.